CANCER IMMUNOLOGY

Blockade of EGFR improves responsiveness to PD-1 blockade in *EGFR*-mutated non–small cell lung cancer

Eri Sugiyama[1,2]*, Yosuke Togashi[2]*, Yoshiko Takeuchi[2], Sayoko Shinya[2], Yasuko Tada[2], Keisuke Kataoka[3], Kenta Tane[4], Eiichi Sato[5], Genichiro Ishii[6], Koichi Goto[7], Yasushi Shintani[8], Meinoshin Okumura[8], Masahiro Tsuboi[4], Hiroyoshi Nishikawa[1,2]†

The clinical efficacy of anti–PD-1 (programmed cell death–1) monoclonal antibody (mAb) against cancers with oncogenic driver gene mutations, which often harbor a low tumor mutation burden, is variable, suggesting different contributions of each driver mutation to immune responses. Here, we investigated the immunological phenotypes in the tumor microenvironment (TME) of epidermal growth factor receptor (*EGFR*)–mutated lung adenocarcinomas, for which anti–PD-1 mAb is largely ineffective. Whereas *EGFR*-mutated lung adenocarcinomas had a noninflamed TME, CD4$^+$ effector regulatory T cells, which are generally present in the inflamed TME, showed high infiltration. The EGFR signal activated cJun/cJun N-terminal kinase and reduced interferon regulatory factor–1; the former increased CCL22, which recruits CD4$^+$ regulatory T cells, and the latter decreased CXCL10 and CCL5, which induce CD8$^+$ T cell infiltration. The EGFR inhibitor erlotinib decreased CD4$^+$ effector regulatory T cells infiltration in the TME and in combination with anti–PD-1 mAb showed better antitumor effects than either treatment alone. Our results suggest that EGFR inhibitors when used in conjunction with anti–PD-1 mAb could increase the efficacy of immunotherapy in lung adenocarcinomas.

INTRODUCTION

Lung cancer, in which about 80% of cases are classified as non–small cell lung cancer (NSCLC), is one of the leading causes of cancer-related mortality worldwide. Alterations in several oncogenic driver genes, including genes encoding epidermal growth factor receptor (*EGFR*) and anaplastic lymphoma kinase (*ALK*), have been reported in NSCLC. Molecular-targeted therapies directed against these driver gene alterations have been successfully developed, resulting in the improvement of patient prognosis (*1, 2*). The activating *EGFR* mutation is found in 50% of lung adenocarcinomas (LUADs) in East Asia, including Japan (*3*). Although patients with *EGFR* mutations initially respond to EGFR tyrosine kinase inhibitors, they usually become resistant to the therapy later. Thus, effective treatment strategies are urgently needed.

Recently, immune checkpoint blockade (ICB), including monoclonal antibodies (mAbs) against programmed cell death–1 (PD-1) and programmed cell death-ligand 1 (PD-L1), has demonstrated impressive antitumor effects in NSCLC, opening a new era in NSCLC treatment (*4, 5*). However, the efficacy is less than 50%, and development of treatments with increased efficacy is needed. Several approaches have been developed to augment the clinical efficacy of cancer immunotherapy, e.g., combination with chemotherapy, anti–

vascular EGF (VEGF) therapies, other ICBs, and regulatory T cell (T$_{reg}$)–targeted therapies (*6*). Despite the promising results of ICB in NSCLC, a low clinical efficacy of anti–PD-1/PD-L1 mAbs against *EGFR*-mutated NSCLC has been reported (*4, 7, 8*). A retrospective study revealed that *EGFR*-mutated NSCLC has low expression rates of PD-L1, a predictive biomarker, and CD8$^+$ tumor-infiltrating lymphocytes (TILs) (*7*). In contrast, other studies have shown that *EGFR*-mutated NSCLC cell lines have higher PD-L1 expression than *EGFR* wild-type NSCLC cell lines (*9, 10*).

Cancer cells with inherent genetic instability generate abnormal proteins, which have not been previously recognized by the immune system and become immunogenic antigens (neoantigens), thereby spontaneously triggering CD8$^+$ T cell responses that contribute to elimination of the cancer cells from the hosts (*11*). To avoid immune cell attack, cancer cells establish immune-suppressive networks in the tumor microenvironment (TME), resulting in inflamed tumors characterized by concomitant infiltration of CD8$^+$ T cells and immune-suppressive cells, such as T$_{reg}$s and myeloid-derived suppressor cells (MDSCs) (*6*). However, poorly immunogenic cancer cells that are selected during cancer development harbor low levels of neoantigens derived from gene alterations, leading to noninflamed tumors lacking both CD8$^+$ T cells and immune-suppressive cells.

Cancers with oncogenic driver gene mutations, such as *EGFR* mutations, generally have a lower tumor mutation burden than cancers without these mutations, resulting in the development of a noninflamed TME (e.g., low levels of CD8$^+$ T cells and immune-suppressive cells) (*12, 13*). In this study, we explored the immunological status of the TME in *EGFR*-mutated LUADs and identified an intriguing immunological status: high T$_{reg}$ infiltration without CD8$^+$ T cell infiltration, which established a strong noninflamed TME. The intense noninflamed TME was attributed to the downstream signals of *EGFR* mutations that directly controlled T cell infiltration by changing the chemokine milieu in the TME. Therefore,

[1]Department of Immunology, Nagoya University Graduate School of Medicine, Nagoya 466-8550, Japan. [2]Division of Cancer Immunology, Research Institute/Exploratory Oncology Research & Clinical Trial Center (EPOC), National Cancer Center, Chiba 277-8577, Japan. [3]Division of Molecular Oncology, Research Institute, National Cancer Center, Tokyo 104-0045, Japan. [4]Division of Thoracic Surgery, [5]Department of Pathology, Institute of Medical Science, Tokyo Medical University, Tokyo 160-0023, Japan. [6]Division of Pathology, [7]Division of Thoracic Oncology, National Cancer Center Hospital East, Chiba 277-8577, Japan. [8]Department of General Thoracic Surgery, Osaka University Graduate School of Medicine, Osaka 565-0871, Japan.
*These authors contributed equally to this work.
†Corresponding author. Email: hnishika@ncc.go.jp

researchers should develop optimal cancer immunotherapy based on the immune phenotypes in the TME.

RESULTS

PD-L1 expression does not play an important role in preventing antitumor immune responses in *EGFR*-mutated LUADs

PD-L1 expression by tumor cells reduces effector T cell activity and promotes tumor progression (*14*). We first examined whether *EGFR*-mutated NSCLC cells had higher PD-L1 expression than *EGFR* wild-type NSCLC cells. Four cell lines (two *EGFR*-mutated and two *EGFR* wild-type NSCLC cell lines) were prepared from regular cultures without any stimulation, such as cytokines, and *CD274* (encoding PD-L1) expression was examined. *CD274* expression was higher in the *EGFR*-mutated NSCLC cell lines than in the *EGFR* wild-type NSCLC cell lines (fig. S1). To reflect the TME where tumor cells are exposed to interferon-γ (IFN-γ) produced by T cells and other immune cells, we added IFN-γ to the cultures of these NSCLC cell lines. *CD274* expression was strongly elevated in both *EGFR*-mutated and *EGFR* wild-type NSCLC cell lines, resulting in comparable *CD274* expression levels (fig. S1).

In addition, surgically resected tumor specimens from 19 patients with LUADs in which *EGFR* gene status had already been evaluated (6 *EGFR*-mutated and 13 *EGFR* wild-type LUADs) were subjected to RNA sequencing (RNA-seq). *CD274* expression tended to be higher in *EGFR* wild-type LUAD than in *EGFR*-mutated LUAD, which was confirmed by immunohistochemistry (IHC), although the results were not significant (Fig. 1, A to C, and fig. S2). A dataset from The Cancer Genome Atlas (TCGA) also confirmed this trend (fig. S2). Thus, high PD-L1 expression in *EGFR*-mutated NSCLC cell lines, which has been shown in several previous reports (*9, 10*), did not reflect the TME in human NSCLCs and was not a major factor in raising antitumor immune responses in *EGFR*-mutated LUADs.

Immune-related gene expression and tumor mutation burden are decreased in *EGFR*-mutated LUADs

Nineteen LUAD samples subjected to RNA-seq were clustered on the basis of gene sets [CD4$^+$ T$_{regs}$, CD8$^+$ T cells, macrophages, dendritic cells (DCs), major histocompatibility complex (MHC) class I, costimulatory antigen-presenting cells (APCs) and T cells, coinhibitory APCs and T cells, IFN response, and cytolytic activity] (*12*); 6 samples were inflamed (i.e., high-CD8$^+$ T cell genes and high–cytolytic activity genes), and 13 samples were noninflamed (Fig. 1A). Of 13 noninflamed samples, 6 were *EGFR*-mutated LUADs, whereas all 6 inflamed samples were *EGFR* wild-type LUADs. *EGFR*-mutated LUADs showed substantially lower *CD274*, *PDCD1* (encoding PD-1), *CD8A*, *GZMA*, and *PRF1* expression than *EGFR* wild-type LUADs (Fig. 1B and fig. S2). There was no significant difference in smoking status, stage, or tumor size between the inflamed and noninflamed samples (Fig. 1A).

Next, whole-exome sequencing was performed with LUAD samples from which sufficient DNA samples were available. Both non-synonymous single-nucleotide variants and frameshift mutations, which can reflect the number of gene alteration-associated neoantigens and are associated with clinical efficacy of anti–PD-1 mAbs (*11*), were significantly higher in *EGFR* wild-type LUADs than in *EGFR*-mutated LUADs (Fig. 1D). TCGA data also confirmed the higher immune-related gene expression and tumor mutation burden in

EGFR wild-type LUADs than mutated LUADs (fig. S2). These findings suggest that *EGFR*-mutated LUADs have a noninflamed TME with a low tumor mutation burden.

### Increased prevalence of T$_{regs}$ in *EGFR*-mutated LUADs

In addition to gene assays of our 19 LUAD samples and TCGA data, flow cytometry and/or cytometry by time of flight (CyTOF) assays with TILs collected from 26 surgically resected LUADs (7 *EGFR*-mutated and 19 *EGFR* wild-type LUADs) were performed for detailed immune profiling of the TME. In *EGFR*-mutated LUADs, the frequency of CD8$^+$ T cells was lower than that of the *EGFR* wild-type LUADs in CyTOF, consistent with the RNA-seq results. In addition, activated PD-1$^+$CD8$^+$ T cell and Gzmb$^+$CD8$^+$ T cell fractions were reduced in *EGFR*-mutated LUADs (Fig. 2A and fig. S3). FOXP3$^+$CD4$^+$ T$_{regs}$, which are generally accompanied by effector T cells such as CD8$^+$ T cells (*15*), were highly detected in *EGFR*-mutated LUADs (Fig. 2A).

To validate these data, we also investigated TILs with flow cytometry. Correct identification of T$_{regs}$ in humans is compromised because of the up-regulation of FOXP3 upon T cell receptor stimulation in conventional T cells (*16*). We have therefore proposed a classification of human T$_{regs}$ based on the expression levels of a naive marker CD45RA and FOXP3, and FOXP3$^+$CD4$^+$ T cells can be divided into three fractions: naive T$_{regs}$ (fraction I: nT$_{regs}$, CD45RA$^+$FOXP3^{low}CD4$^+$); effector T$_{regs}$ (fraction II: eT$_{regs}$, CD45RA$^-$FOXP3^{high}CD4$^+$), with strong immune suppressive functions; and non-T$_{regs}$ (fraction III: CD45RA$^-$FOXP3^{low}CD4$^+$) without suppressive functions (Fig. 2B) (*17–19*). TIL analyses with flow cytometry confirmed that the frequency of CD8$^+$ T cells tended to be lower in *EGFR*-mutated LUADs than in *EGFR* wild-type LUADs (Fig. 2B). The frequency of tumor-infiltrating eT$_{regs}$ and the eT$_{reg}$/CD8$^+$ T cell ratio were significantly higher in *EGFR*-mutated LUADs than in *EGFR* wild-type LUADs, corresponding to the data from CyTOF and IHC (Figs. 1C and 2, A, and B). These findings suggest that T$_{regs}$ infiltrate into the TME despite the low levels of CD8$^+$ effector T cells in *EGFR*-mutated LUADs. In contrast, only 2 of 19 patients with *EGFR* wild-type LUADs (AD no. 15 and no. 16) had a high eT$_{reg}$/CD8$^+$ T cell ratio (>0.2) (Fig. 2B), and *FOXP3* expression in these patients was very high in accordance with the inflamed TME (Fig. 1A and fig. S2). Such patients seemed to have "inflammation-related acquired T$_{regs}$" in the TME, and indeed, the *FOXP3* gene, a representative T$_{reg}$-related gene, was clustered into inflamed gene sets (Fig. 1A and fig. S4A) (*15*). There was no significant correlation between smoking status, stage, or tumor size and CD8$^+$ T cell or eT$_{reg}$ infiltration (fig. S5).

In addition to T$_{reg}$ infiltration, tumor-associated macrophages (TAMs; CD68$^+$CD163$^+$CD206$^+$ cells), MDSCs (CD33$^+$CD11b$^+$ cells), and DCs (CD11c$^+$CD11b$^-$HLA-DR$^+$ cells) were analyzed with multi-plex fluorescent IHC. In *EGFR*-mutated LUADs, the frequencies of TAMs, MDSCs, and DCs tended to be slightly, but not significantly, higher than those of *EGFR* wild-type LUADs, which is consistent with the RNA-seq data (Fig. 1A and fig. S6).

Chemokine changes by EGFR signals are associated with the immune phenotypes in *EGFR*-mutated LUADs

To gain insight into the mechanism(s) for this immunological status of *EGFR*-mutated LUADs (high T$_{reg}$ infiltration despite low CD8$^+$ effector T cell infiltration), we investigated the effect of EGFR signaling on CD8$^+$ effector T cells and T$_{reg}$ infiltration with two *EGFR*-mutated cell lines (PC-9 and HCC827) and an *EGFR* wild-type cell line (H322) treated with erlotinib and EGF, respectively. Comprehensive
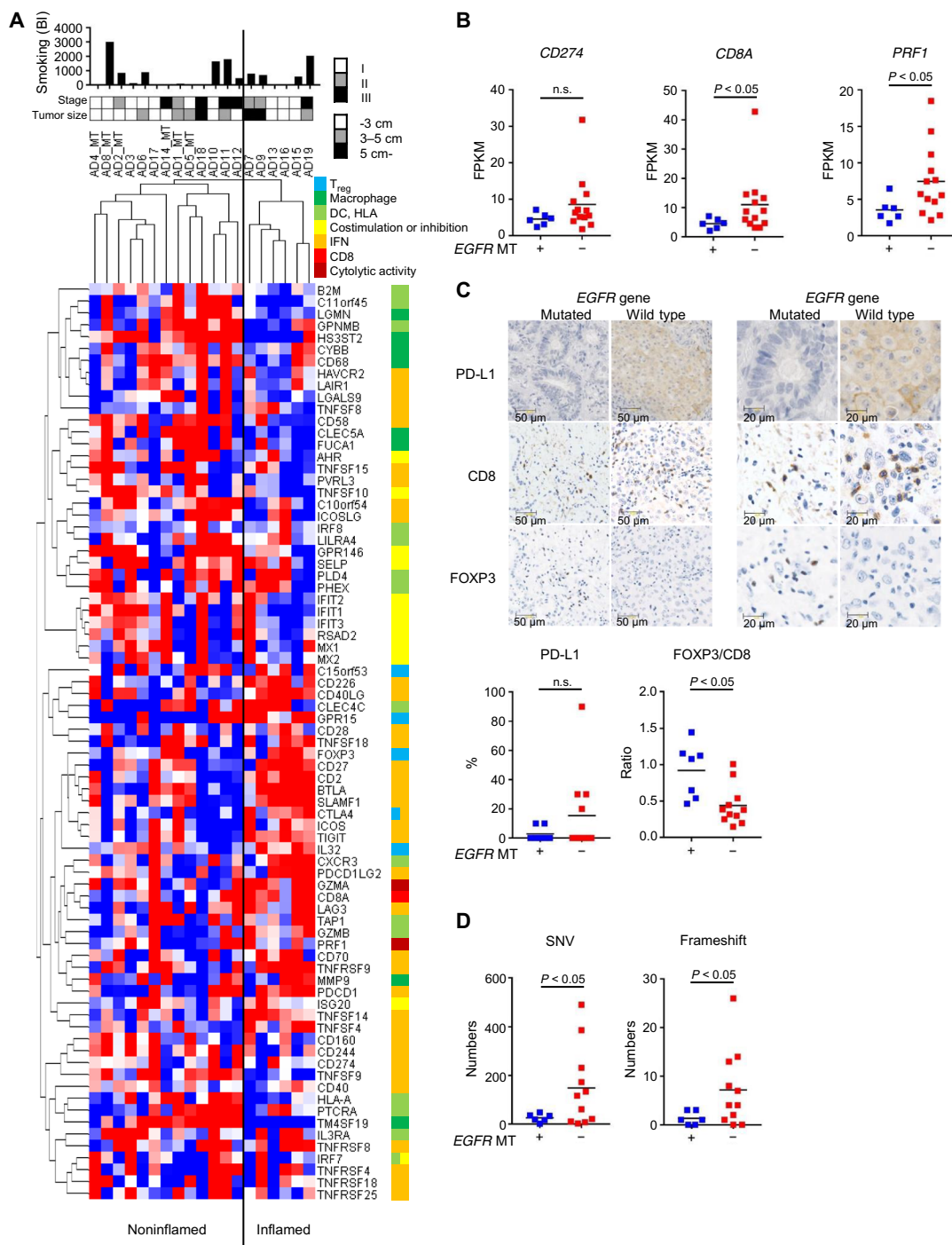
Fig. 1. Immune-related gene expression and tumor mutation burden are decreased in *EGFR*-mutated LUADs. (**A**) Heatmap of RNA-seq from surgically resected LUADs. Nineteen LUAD samples were subjected to RNA-seq and clustered by previously reported gene sets (CD4+ T_regs, CD8+ T cells, macrophages, DCs, MHC class I, costimulatory APCs and T cells, coinhibitory APCs and T cells, IFN response, and cytolytic activity) (*11*). MT, *EGFR*-mutated; BI, Brinkman index. (**B**) Gene expression of *CD274*, *CD8A*, and *PRF1* according to *EGFR* gene status. n.s., not significant. (**C**) Representative IHC for PD-L1, CD8, and FOXP3 according to *EGFR* gene status (top). Summary of PD-L1 expression and the ratio of FOXP3/CD8 (bottom). (**D**) Tumor mutation burden according to *EGFR* gene status. Both single-nucleotide variants (SNV) and frameshift mutations were examined.

chemokine production, was commonly enriched in the down-regulated state of the EGFR signal (fig. S7). Consistently, we found that gene ontology (GO) terms, cytokines, and chemokines, such as *CCL5* and *CXCL10*, which reportedly recruit CD8+ T cells (*20*, *21*), were down-regulated by EGFR signaling (Fig. 3A). In addition, *CCL22*, which recruits T_regs (*19*, *22*, *23*), was elevated with activation of EGFR signaling (*EGFR*-mutated cell lines without erlotinib and *EGFR* wild-type cell line with EGF) (Fig. 3A). This elevation was abrogated by inhibition of EGFR signaling with an erlotinib in *EGFR*-mutated cell lines. The changes in mRNA and protein expression were observed with both erlotinib and third-generation EGFR tyrosine kinase inhibitor (osimertinib), as shown by quantitative real-time reverse transcription polymerase chain reaction (qRT-PCR) and by enzyme-linked immunosorbent assay (ELISAs) (Fig. 3, B and C, and figs. S8 and S9).

EGFR signaling controls the transcription factors JNK/cJUN and IRF1 for the immune phenotype of *EGFR*-mutated LUADs

To further examine chemokine changes by EGFR signaling, we analyzed the transcriptional regulation of these chemokines. Because the *JNK* (cJun N-terminal kinase)/*cJun* pathway has been reported to increase *CCL22* expression (*24*), *JUN* expression was examined. *JUN* expression was augmented along with *CCL22* expression (Fig.4, A and B). The increases in cJUN and phospho-cJUN were induced by phospho-JNK via EGFR signaling (Fig. 4C). In addition, *JUN* knockdown decreased *CCL22* expression but not *CXCL10* expression (Fig. 4D). A luciferase assay using *CCL22* promoter regions

gene expression was analyzed with a microarray, and gene set enrichment analysis (GSEA) revealed that the gene signature of INTERFERON_GAMMA_RESPONSE, which is associated with

duced by phospho-JNK via EGFR signaling (Fig. 4C). In addition, *JUN* knockdown decreased *CCL22* expression but not *CXCL10* expression (Fig. 4D). A luciferase assay using *CCL22* promoter regions
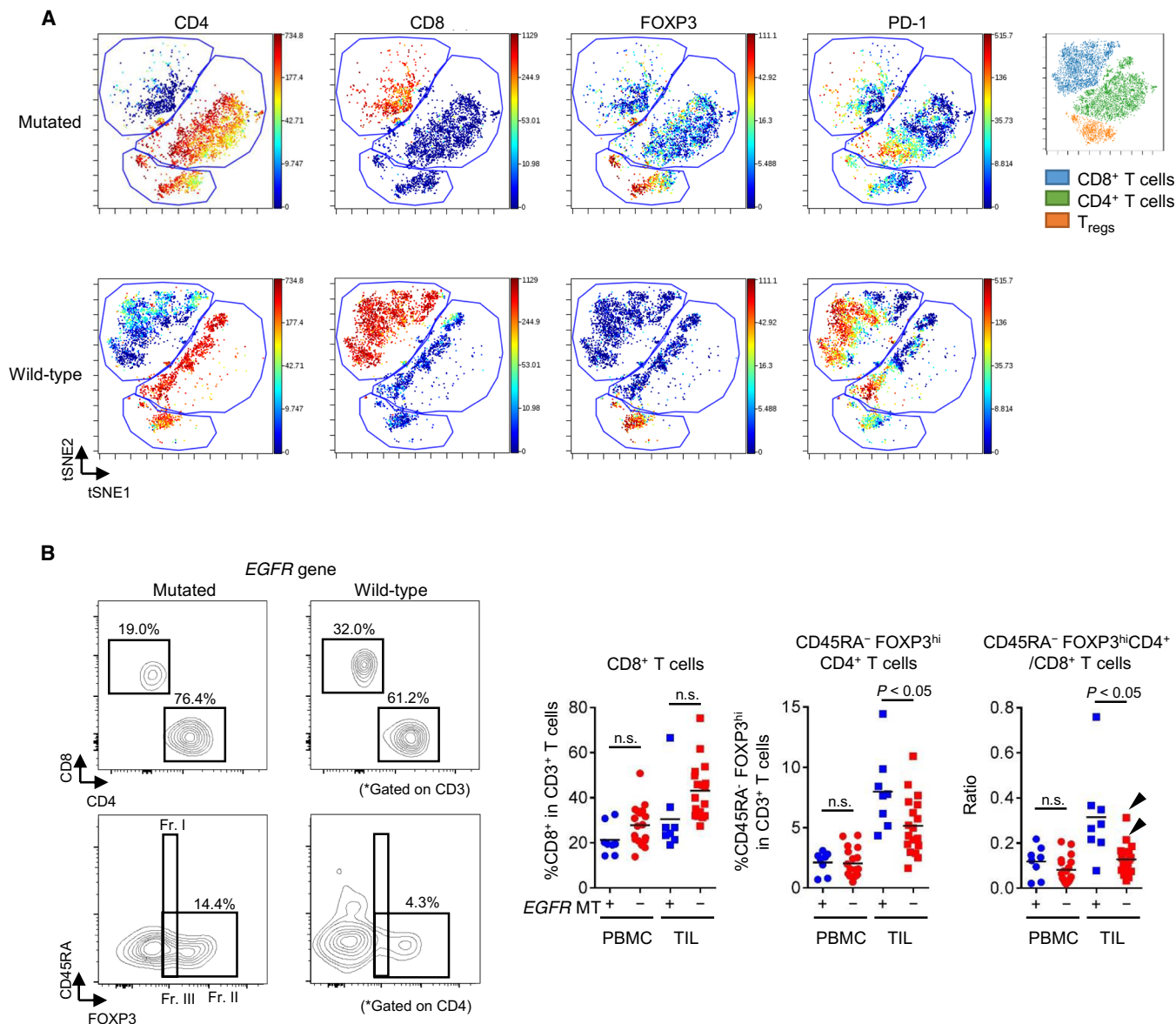
Fig. 2. T$_{regs}$ highly infiltrate into *EGFR*-mutated LUADs with a noninflamed TME. (A) TILs from *EGFR*-mutated and wild-type LUADs were subjected to CyTOF assays, and representative tSNE plots (CD4, CD8, FOXP3, and PD-1) are shown. **(B)** Left: Representative flow cytometry staining (CD4/CD8 for T cells and CD45RA/FOXP3 for CD4$^+$ T cells) of TILs from *EGFR*-mutated and wild-type LUADs. Right: Summary of the frequency of the indicated T cell fractions in surgically resected LUADs. Fr. I, fraction I (naive T$_{regs}$); Fr. II, fraction II (effector T$_{regs}$); Fr. III, fraction III (non-T$_{regs}$); *EGFR* MT, *EGFR* mutations.

also demonstrated that *JUN* knockdown decreased *CCL22* luciferase activity (Fig. 4D), suggesting that EGFR signaling increases *CCL22* expression via *JNK/cJun* activation.

To investigate the mechanism(s) of *CCL5* and *CXCL10* reduction, we examined a transcription factor(s) that showed comparable changes to *CXCL10* in the microarray data. We found that *interferon regulatory factor 1* (*IRF1*) expression was concurrently changed with *CXCL10* expression (Fig. 4A) and was down-regulated by the activation of EGFR signaling (Fig. 4, A and B). The phosphatidylinositol 3-kinase/AKT pathway, which is downstream of the EGFR signal, has been reported to inhibit IRF1 expression (*25*, *26*). Accordingly, pAKT was increased by the activation of the EGFR signal, consequently decreasing IRF1 (Fig. 4C). In addition, *IRF1* knockdown resulted in

the down-regulation of *CXCL10*, but not *CCL22*, at the mRNA level and in luciferase assays (Fig. 4E), indicating that the EGFR signaling decreased *CXCL10* expression via *IRF1* inhibition. We propose that the EGFR signaling plays an important role in driving high T$_{reg}$ infiltration despite low CD8$^+$ effector T cell infiltration in *EGFR*-mutated LUADs via *CCL22* up-regulation through *JNK/cJun* and *CXCL10* down-regulation mediated by *IRF1* (Fig. S4B).

A combination with erlotinib and anti–PD-1 mAb is a potential treatment strategy for *EGFR*-mutated LUADs

The functions of immune cells expressing EGFR might be directly modified the by EGFR tyrosine kinase inhibitor (*27*, *28*). To evaluate the direct effect of erlotinib on CD8$^+$ T cells and T$_{regs}$, we
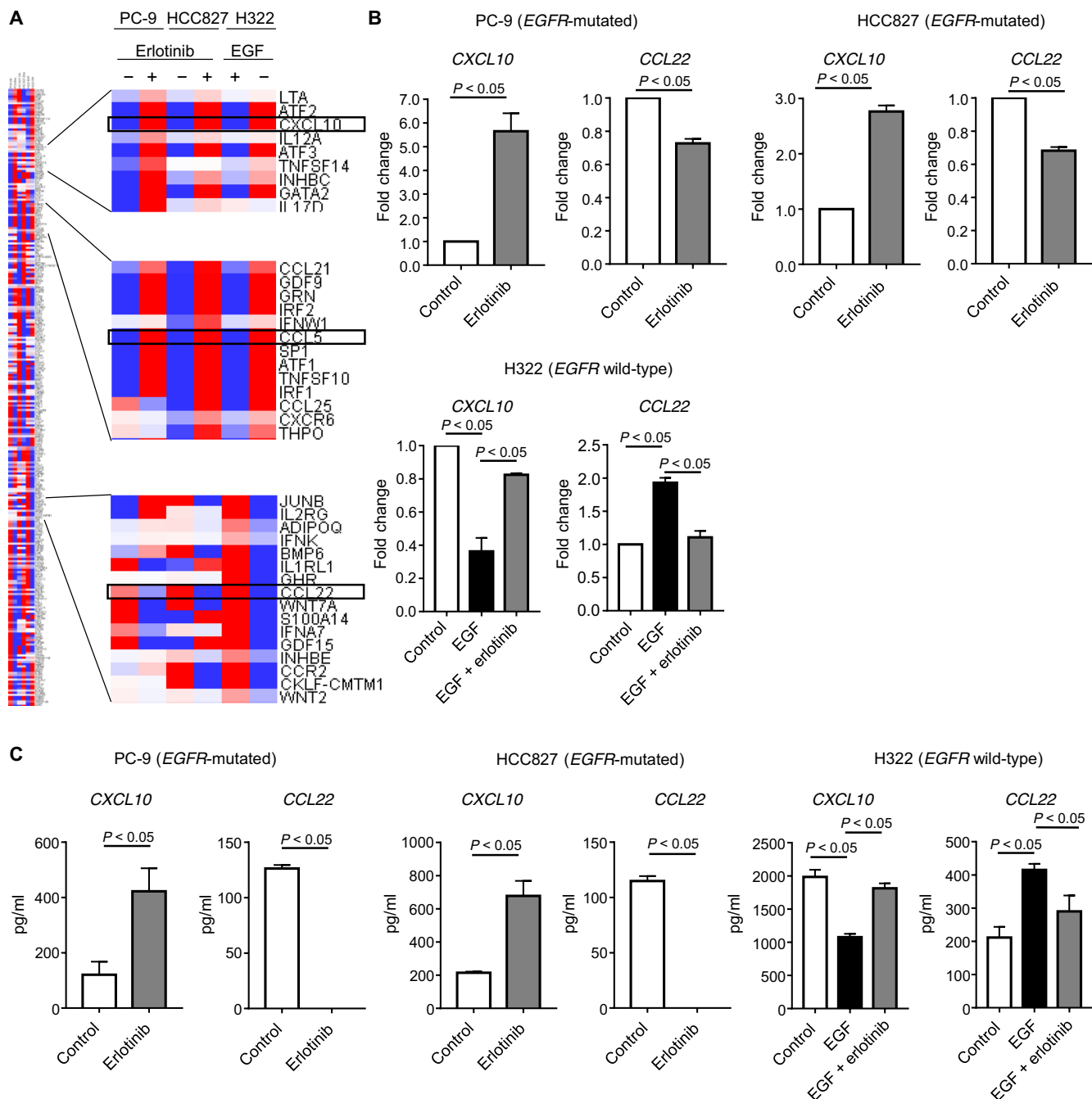
Fig. 3. CXCL10 recruiting CD8+ effector T cells is down-regulated and CCL22 recruiting T_regs is up-regulated by EGFR signal in _EGFR_-mutated LUADs. (**A**) Two _EGFR_-mutated cell lines (PC-9 and HCC827) and an _EGFR_ wild-type cell line (H322) treated with erlotinib and EGF, respectively, were subjected to microarray analysis. GO terms, cytokines, and chemokines were examined. (**B**) _CXCL10_ and _CCL22_ expression levels in the _EGFR_-mutated cell lines (PC-9 and HCC827) treated with and without erlotinib and the _EGFR_ wild-type cell line (H322) treated with and without EGF and erlotinib were evaluated by qRT-PCR. (**C**) The concentrations of CXCL10 and CCL22 in the cultured medium of the _EGFR_-mutated cell lines (PC-9 and HCC827) treated with and without erlotinib and the _EGFR_ wild-type cell line (H322) treated with and without EGF and erlotinib were examined by ELISAs. Data are shown from three independent experiments.

analyzed EGFR expression by immune cells in peripheral blood mononuclear cell (PBMC) and their sensitivity to erlotinib. Immune cells, including CD8+ T cells and T_regs, had limited expression of EGFR compared with lung cancer cell line PC-9 (fig. S10A). Accordingly, both CD8+ T cells and T_regs failed to respond to erlotinib treatment (fig. S10, B and C). In addition, phospho–

Janus kinase 2 (pJAK2) and phospho–signal transducer and activator of transcription 5 (pSTAT5), which are downstream of the EGFR signal in immune cells (_29_), were not altered, and the expression levels of chemokines (_CXCL10_, _CCL5_, and _CCL22_) and transcription factors (_IRF1_ and _JUN_) were not changed (fig. S10, D and E). These findings indicate that the EGFR signal does not

Fig. 4. EGFR signaling controls the transcription factors *JNK/cJUN* and *IRF1* for the immune phenotype of *EGFR*-mutated LUADs. (A) Two *EGFR*-mutated cell lines (PC-9 and HCC827) and an *EGFR* wild-type cell line (H322) treated with erlotinib and EGF, respectively, were subjected to microarray analysis. The expression of transcription factors was examined. **(B)** *JUN* and *IRF1* expression in the *EGFR*-mutated cell lines (PC-9 and HCC827) with and without erlotinib, and the *EGFR* wild-type cell line (H322) treated with and without EGF and erlotinib were evaluated by qRT-PCR. **(C)** PC-9 (*EGFR*-mutated cell line) treated with and without erlotinib and H322 (*EGFR* wild-type cell line) were treated with and without EGF and erlotinib, and transcription factor expression was examined with Western blotting. **(D)** Left: *JUN* expression by PC-9 was knocked down by siRNA, and protein expression was confirmed with Western blotting. Right: *CXCL10* and *CCL22* gene expression was examined by qRT-PCR, and luciferase activity of the *CXCL10* and *CCL22* promoter regions was examined by luciferase assays. **(E)** *IRF1* expression by PC-9 was knocked down by siRNA, and protein expression was confirmed with Western blotting. Right: *CXCL10* and *CCL22* gene expression was examined by qRT-PCR, and luciferase activity of the *CXCL10* and *CCL22* promoter regions was examined by luciferase assays. Data from three independent experiments are shown.
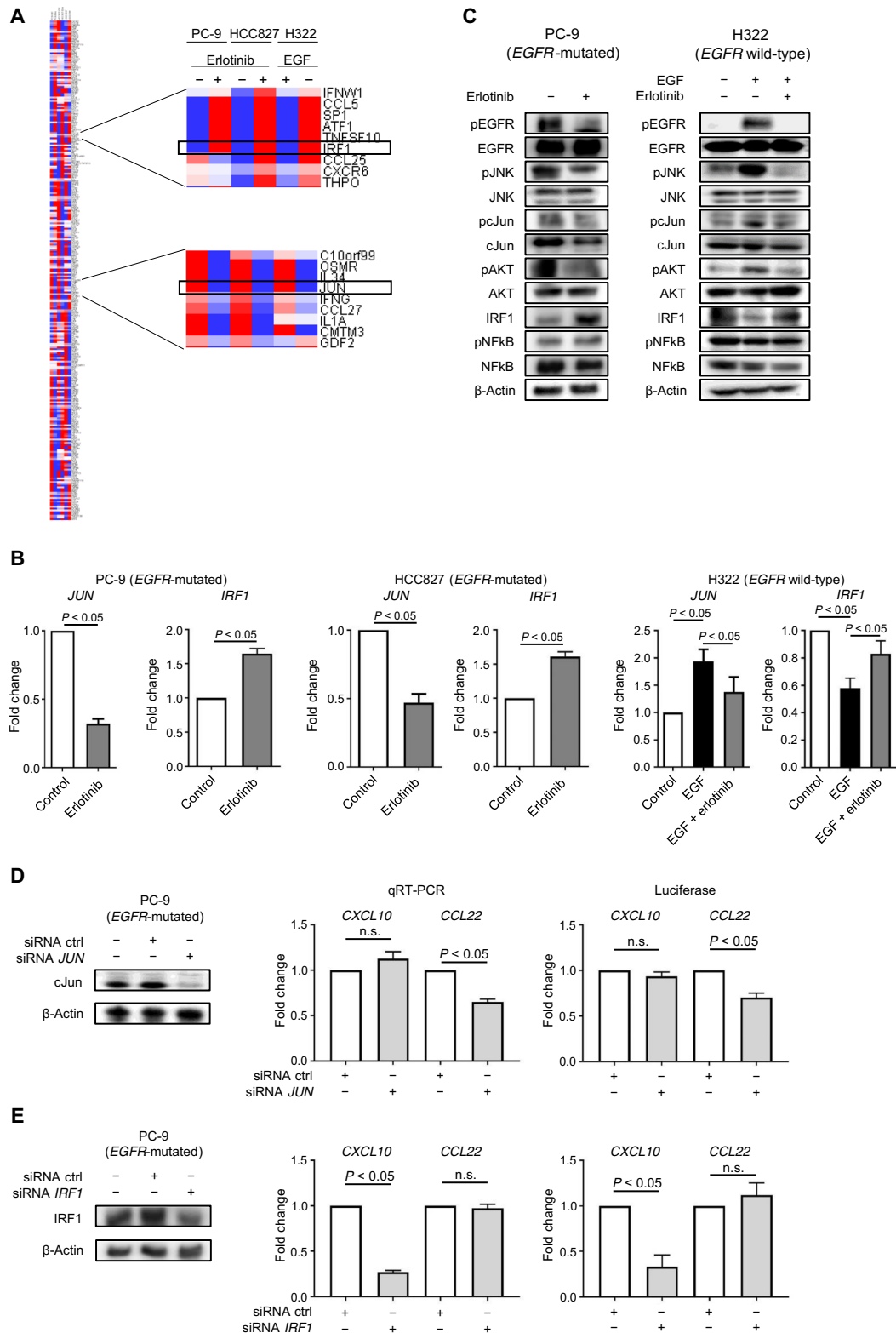
directly influence on CD8$^+$ T cells and T$_{regs}$.

We next addressed whether EGFR signal inhibition altered the immunological status (high T$_{reg}$ infiltration despite low CD8$^+$ effector T cell infiltration) of *EGFR*-mutated LUADs and prevented tumor growth/progression. T$_{reg}$ frequency in the TME of patients with *EGFR*-mutated LUADs who received erlotinib treatment was examined. T$_{reg}$ infiltration was significantly reduced after erlotinib treatment (Fig. 5A), suggesting that a combination treatment with erlotinib and anti–PD-1 mAb could be possible. *CXCL10* expression tended to be higher and *CCL22* expression tended to be lower after erlotinib treatment than before erlotinib treatment in patients with *EGFR*-mutated LUADs, although there

was no significant difference due to the small size of our patient cohort (fig. S11).

We then used human *EGFR* mutant (exon 19 deletion)–transfected mouse cell lines, a bulk cell line after transfection and two single

Fig. 5. The combination treatment with erlotinib and anti–PD-1 mAb effectively induces tumor growth inhibition in *EGFR*-mutated LUADs. (**A**) Left: Representative flow cytometry staining (CD45RA/FOXP3 for CD4^{+} T cells) of TILs. Right: A summary of patients with advanced LUAD treated with EGFR tyrosine kinase inhibitors (TKIs). TILs were collected before and after EGFR tyrosine kinase inhibitor treatment and subjected to flow cytometry. (**B**) Human *EGFR* wild-type or mutant (exon 19 deletion)–transfected MC-38 mouse cell line (MC-38wt or MC-38ex19del, respectively) was established, and human EGFR expression, phospho-EGFR, and exon 19-deleted EGFR were confirmed by Western blotting. (**C**) Mice were inoculated with MC-38wt or MC-38ex19del with and without erlotinib treatment, and tumor-infiltrating T$_{regs}$ and CD8^{+} T cells were analyzed. Left: Representative flow cytometry staining of TILs. Right: A summary of the frequency of FOXP3^{+}CD4^{+} T cells and CD8^{+} T cells and ratio of FOXP3/CD8. (**D**) CXCL10, CCL22, CCL5, IRF1, and JUN expression levels in MC-38wt and MC-38ex19del with and without erlotinib were evaluated by qRT-PCR. Mice were inoculated with MC-38wt or MC-38ex19del with and without erlotinib treatment. Tumors were collected on day 8, and CXCL10, CCL22, CCL5, IRF1, and JUN expression was analyzed with qRT-PCR. (**E**) Mice were inoculated with MC-38mock or MC-38wt or MC-38ex19del and treated with and without erlotinib, anti–PD-1 mAb, or the combination (erlotinib + anti–PD-1 mAb). Tumor growth and the survival curve are shown. Representative data from two independent experiments are shown. (**F**) Human *EGFR* wild-type or mutant (exon 19 deletion)–transfected LL/2-OVA mouse cell line (LL/2-OVAwt or LL/2-OVAex19del, respectively) was established, and human EGFR expression, phospho-EGFR, and exon 19–deleted EGFR were confirmed by Western blotting. (**G**) Mice were intravenously administered with LL/2-OVAex19del and treated with and without erlotinib, anti–PD-1 mAb or a combination (erlotinib + anti–PD-1 mAb). A summary of lung weights with tumors is shown. Representative data are shown from two independent experiments.
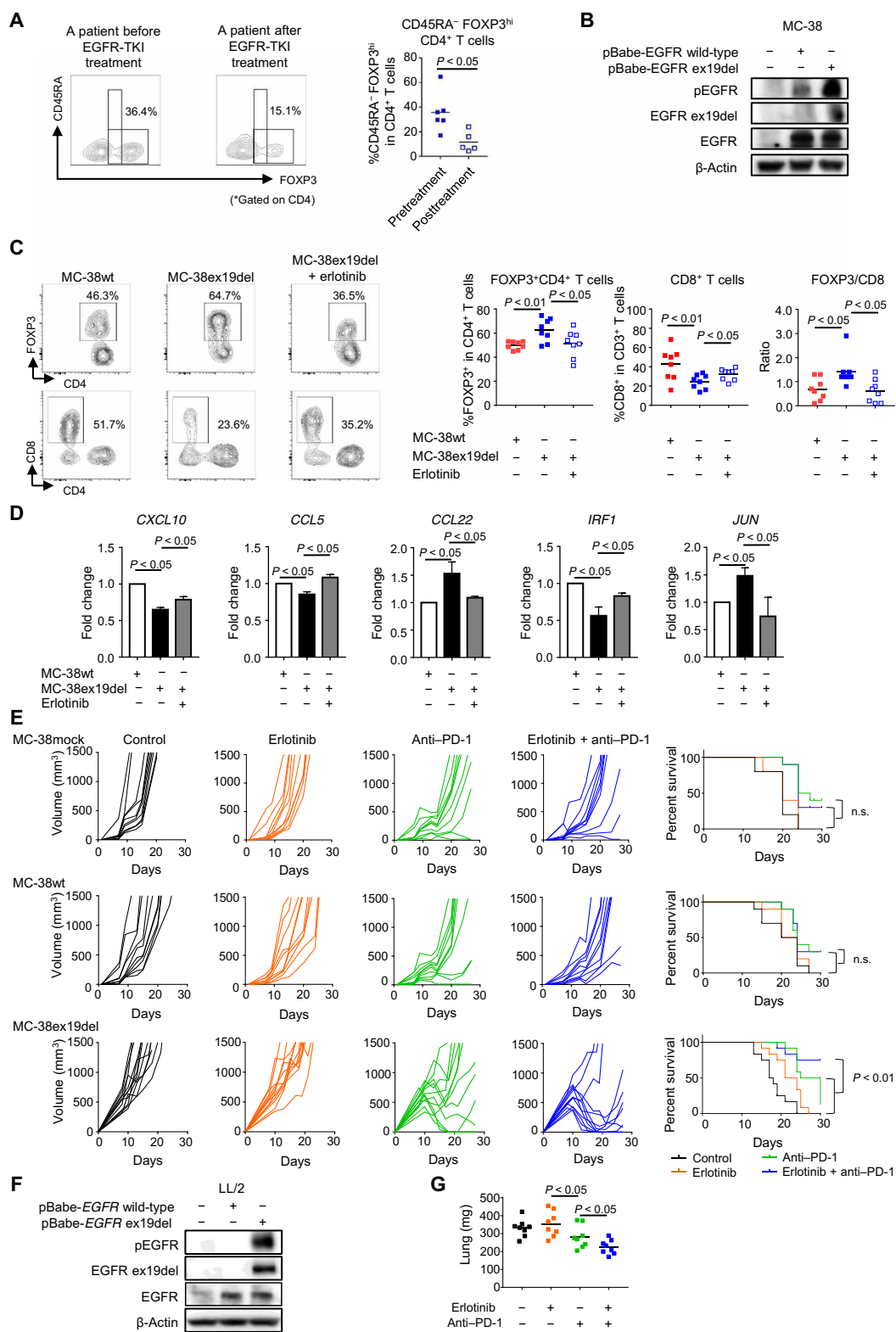
clones of MC-38ex19del, to examine the in vivo antitumor activity (Fig. 5B and figs. S12A and S13). Compared with those of *EGFR* wild-type transfected cell line (MC-38wt)–derived tumors, higher and lower frequencies of T$_{regs}$ and CD8^{+} T cells, respectively, were observed in the TME of MC-38ex19del–derived tumors. The high T$_{reg}$ and low CD8^{+} T cell infiltration in the TME was totally abrogated by erlotinib treatment (Fig. 5C). In addition, consistent changes in chemokines and transcription factors were observed:

CXCL10, *CCL5*, and *IRF1* were down-regulated in MC-38ex19del–derived tumors and were increased by erlotinib treatment. *CCL22* and *JUN* were up-regulated in MC-38ex19del–derived tumors and were reduced by erlotinib treatment (Fig. 5D). Furthermore, when CXCL10 was blocked with an antibody, the elevation of CD8$^+$ T cells in the TME induced by erlotinib treatment was abrogated (fig. S14A), and no synergistic effect of erlotinib and anti-CCL22 mAb on T$_{regs}$ in the TME was observed (fig. S14B). Consequently, the combination of erlotinib and anti–PD-1 mAb significantly inhibited tumor growth compared with the control or either single treatment using a bulk cell line after transfection and two single clones of MC-38ex19del (Fig. 5E and fig. S12B). In contrast, no synergistic effect of erlotinib and anti–PD-1 mAbs was observed in the control cell lines (MC-38mock and MC-38wt) (Fig. 5E). Moreover, this combination treatment exhibited a superior antitumor effect on orthotopic *EGFR* exon 19 deletion–transfected LL/2-OVA (LL/2-OVAex19del; a bulk cell line after transfection) than either treatment alone (Fig. 5, F and G). Additional T$_{reg}$ depletion with anti-CD25 mAb failed to show any synergistic or additive antitumor effects (fig. S15). Our results suggest that combination treatment with an EGFR tyrosine kinase inhibitor such as erlotinib and anti–PD-1 can be a promising strategy for the treatment of *EGFR*-mutated LUADs.

DISCUSSION

Cancers are immunologically divided into two major types, inflamed and noninflamed tumors. T$_{regs}$ have been thought to be recruited by inflammation into the TME ("inflammation-related acquired T$_{reg}$") (fig. S4) (*15*), as was observed in *EGFR* wild-type LUADs. In this study, we identified an intriguing immunological status in *EGFR*-mutated LUADs: high T$_{reg}$ infiltration despite the noninflamed TME. We then proposed a concept of immune suppression, particularly by T$_{regs}$ in the TME, "tumor-related innate T$_{regs}$" (fig. S4). The dependence of tumor growth and/or survival on driver gene alterations such as *EGFR* mutations or *ALK* rearrangements in NSCLC is known as oncogenic driver addiction. Patients with such oncogenic driver gene alterations respond to molecular-targeted therapies (*1*, *2*), indicating an important role of such oncogenic driver gene alterations in cell growth or survival. In addition, we found that these gene alterations play another crucial role in immune responses through development of an immune-suppressive environment in the TME of *EGFR*-mutated LUADs. Together, driver genes contribute to not only cell growth and/or survival but also immune escape from antitumor immunity.

Several previous studies have demonstrated that *EGFR*-mutated NSCLC cell lines have higher expression of PD-L1, one of the predictive biomarkers of PD-1/PD-L1 blockade therapies (*5*), than *EGFR* wild-type NSCLC cell lines (*9*, *10*). PD-L1 expression is induced by two different mechanisms: genetic alterations (i.e., amplification, fusion, and 3′ untranslated region disruption) (innate expression) and induction by inflammation (such as acquired IFN-γ expression) (*14*). We revealed that whereas *EGFR*-mutated NSCLC cell lines cultured with regular medium without any stimulation, such as cytokines, exhibited slightly higher *CD274* (encoding PD-L1) expression than *EGFR* wild-type NSCLC cell lines, *CD274* expression was strongly enhanced by IFN-γ, showing a strong elevation of *CD274* expression in both *EGFR*-mutated and *EGFR* wild-type NSCLC cell lines regardless of their original expression. The extent of *CD274* elevation induced by IFN-γ was significantly higher in *EGFR* wild-type NSCLC cell lines than in *EGFR*-mutated NSCLC cell lines. *CD274* expression is primarily regulated by IFN-γ via *IRF1* (*30*), and our study revealed that EGFR signaling negatively regulated *IRF1*. Therefore, *IRF1* is suppressed by EGFR signaling in *EGFR*-mutated LUADs, resulting in a low increase in *CD274* expression by IFN-γ. RNA-seq and IHC exhibited higher PD-L1 expression in *EGFR* wild-type LUADs than in *EGFR*-mutated LUADs, and PD-1 blockade resulted in poor clinical responses in *EGFR*-mutated LUADs (*4*, *7*, *8*).

The clinical responses of anti–PD-1/PD-L1 mAbs against *EGFR*-mutated LUADs were unfavorable because of the low tumor mutation burden, low PD-L1 expression, and the noninflamed TME (*7*, *8*). Tumor mutation burden can be reflected in the number of neoantigens derived from gene alterations, which induce a strong immune response as nonself antigens, leading to an inflamed TME. Thus, tumor mutation burden is reportedly associated with the clinical efficacy of anti–PD-1/PD-L1 mAbs (*11*). In our analyses, because tumor mutation burden was low in *EGFR*-mutated LUADs, immune-related gene expression was low in *EGFR*-mutated LUADs. T$_{reg}$ infiltration, which was frequently accompanied by CD8$^+$ T cell infiltration in the inflamed TME (*15*), in *EGFR*-mutated cancers tended to be higher or comparable with that in *EGFR* wild-type cancers, although CD8$^+$ T cell infiltration was limited in *EGFR*-mutated cancers. Therefore, the TME (high T$_{reg}$ infiltration without CD8$^+$ T cell infiltration) was not developed solely because of low tumor mutation burden; rather, the immunological effects of *EGFR* mutations must be strongly involved via prevention of the recruitment of effector CD8$^+$ T cells by down-regulation of *CXCL10* through *IRF1* and promotion of T$_{reg}$ infiltration by up-regulation of *CCL22* through *JNK/cJUN*. Considering that T$_{regs}$ hamper the development of effective antitumor immunity in tumor-bearing hosts (*19*), the immunological status in the TME induced by *EGFR* mutations can be associated with resistance to cancer immunotherapy, as observed in our in vivo study, suggesting that combination treatment of anti–PD-1 mAb and EGFR signal inhibitors should augment the antitumor efficacy. In patients with advanced *EGFR*-mutated LUADs, tumor-infiltrating eT$_{reg}$ frequency was significantly lower after erlotinib treatment. Although several clinical trials of EGFR tyrosine kinase inhibitors in combination with anti–PD-1 mAb have been performed, the high incidence of treatment-related adverse effects limited successful clinical application. In contrast, a recent phase 3 trial demonstrated that anti–PD-L1 antibody combined with bevacizumab, an anti-VEGF therapy, exhibits clinical efficacy against *EGFR*-mutated NSCLC (*31*). Antiangiogenic drugs reportedly reduced T$_{regs}$ (*32*), which can partially explain the superior clinical efficacy of the combination therapy against *EGFR*-mutated NSCLC. However, the tumor mutation burden is lower in *EGFR*-mutated NSCLC than in *EGFR* wild-type NSCLC, indicating smaller numbers of neoantigens. In addition to regulating EGFR signaling, combination strategies that elicit CD8$^+$ T cells against cancer antigens, although the number is limited, may provide notably favorable clinical efficacy in *EGFR*-mutated NSCLC.

Chemokine production is controlled by multiple components, such as tumor cells and immune cells (*33*). Consistent with this finding, the basal level of CCL22 production in the *EGFR* wild-type H322 cell line was higher than in other *EGFR*-mutated cell lines. Inflammatory signals provided in the TME may imprint CCL22 production in the H322 cell line. Therefore, although *CCL22* expression is regulated by the *JNK/cJUN* signal, which is downstream of the EGFR signal in our data, many other signals may regulate

CCL22 expression (*34*). Thus, tumor cell line information may not directly influence the TME. In MC-38 tumor model in which we can directly examine the role of EGFR signaling in *CCL22* expression, MC-38 with an *EGFR* mutation increased *CCL22* expression compared with wild-type MC-38, resulting in enhanced T_{reg} infiltration in the TME. These findings indicated the critical roles of chemokines derived from *EGFR*-mutated cancers in both T_{reg} and $CD8^+$ T cell infiltration in the TME. The other chemokine that showed elevation with EGFR signal activation was *CXCL8*, which reportedly mainly recruited neutrophils (*35*). In contrast, *CCL21* (a ligand of CCR7), which mainly promoted the chemotaxis of natural killer T cells and naive T cells (*36*), respectively, were down-regulated by the EGFR signals, consistent with the noninflamed TME in *EGFR*-mutated cancer (fig. S16). However, consistent tendencies were not observed in the RNA-seq data.

Whereas EGFR expression by immune cells, including T_{regs}, has been detected (*27, 28*), we found limited expression of EGFR in T_{regs} and $CD8^+$ T cells. Accordingly, erlotinib treatment did not influence the viability or function, including chemokines, of these cells. In addition, synergistic antitumor effects by the combination of erlotinib and anti–PD-1 mAb in EGFR wild-type cancers were not observed when compared with that of anti–PD-1 mAb alone. As EGFR expression by T_{regs} was reported in inflammatory conditions (*27*), one plausible explanation is that immune cells, particularly T_{regs}, use various different signals for molecular expression depending on each condition, such as cancers and inflammation. In *EGFR*-mutated cancers, the noninflamed immune-suppressive TME (high T_{regs} and low $CD8^+$ T cells) may reduce the expression of EGFR by immune cells such as T_{regs}.

In conclusion, we found an intriguing immunological status in the TME of *EGFR*-mutated LUADs: high T_{reg} infiltration despite the noninflamed TME. T_{regs} are primarily recruited via signals from tumor cells ("tumor-related innate T_{regs}"), which are induced by driver gene alterations such as *EGFR* mutations and related to resistance to cancer immunotherapies. Driver gene alterations represented by *EGFR* mutations therefore play an important role in cell growth and/or survival and the development of immune escape machineries, warranting further tests in cancer immunotherapies combined with molecular-targeted therapies against cancers with driver gene alterations.

MATERIALS AND METHODS
Patients and samples
Peripheral blood and tumor tissues were obtained from patients with LUADs who underwent surgery at Osaka University Hospital and National Cancer Center Hospital East from 2014 to 2015 and advanced LUAD patients harboring *EGFR* mutations who received EGFR tyrosine kinase inhibitors, such as gefitinib, erlotinib, and afatinib, treatment at National Cancer Center Hospital East from 2015 to 2016 (summarized in tables S1 and S2, respectively). PBMCs were isolated by density gradient centrifugation with Ficoll-Paque (GE Healthcare, Little Chalfont, UK). For collection of TILs, tumor tissues were minced and treated with gentleMACS Dissociator (Miltenyi Biotec, Bergisch Gladbach, Germany) as described previously (*18*). PBMCs from healthy individuals were purchased from Cellular Technology Limited (Cleveland, OH). PBMCs were cultured in RPMI 1640 supplemented with 10% AB serum. PBMCs were cultured with CD3/CD28 Dynabeads (Thermo Fisher Scientific,

Waltham, MA) according to the manufacturer's instructions for 3 days. All donors provided written informed consent before sampling, according to the Declaration of Helsinki. This study was performed in a blinded and nonrandomized manner and was approved by Osaka University Hospital Ethics Committee and National Cancer Center Ethics Committee.

IHC for PD-L1, CD8, and FOXP3
The antibodies used in IHC are summarized in table S3. Surgically resected samples were formalin fixed, paraffin embedded, and sectioned onto slides for IHC. The slides were deparaffinized with xylene, rehydrated, and antigen-retrieved in a microwave oven for 20 min. After the inhibition of endogenous peroxidase activity, individual slides were then incubated overnight at 4°C with a mouse anti-human CD8 mAb, a rabbit anti-human FOXP3 mAb, and a rabbit anti-human PD-L1 mAb. The slides were then incubated with EnVision reagent (Dako, Glostrup, Denmark), and a color reaction was developed in 2% 3,3-diaminobenzidine in 50 mM tris buffer (pH 7.6) containing 0.3% hydrogen peroxidase. Last, these sections were counterstained with Meyer hematoxylin. PD-L1 positivity was evaluated in the tumor cells. CD8 and FOXP3 staining was quantified in five high-power microscopic fields (×400; 0.0625 mm^2), and the mean values were calculated. Two pathological researchers (E. Sugiyama and G.I.) independently evaluated the stained slides.

Multiplex immunofluorescence staining
The antibodies used in multiplex immunofluorescence staining are also described in table S3. Surgically resected samples were formalin fixed, paraffin embedded, and sectioned onto slides. The slides were deparaffinized with xylene, rehydrated, and antigen-retrieved in a microwave oven for 40 min. After the inhibition of endogenous peroxidase activity, individual slides were then incubated for 1 hour at room temperature with a rabbit anti-human CD33 mAb, a rabbit anti-human CD11b mAb, a rabbit anti-human CD11c mAb, a mouse anti-human CD68 mAb, a mouse anti-human CD163 mAb, a mouse anti-human CD206 mAb, and a rabbit anti-human HLA-DR mAb. Anti-rabbit/mouse polymeric horseradish peroxidase (System-HRP–labeled polymer anti-rabbit, EnVision, Dako) was applied as the secondary label for 20 min. Signals from the antibody complexes were visualized with their corresponding Opal Fluorophore Reagents (PerkinElmer, Waltham, MA) after incubation of the slides for 10 min. Slides were air-dried, mounted with ProLong Diamond Antifade mounting medium (Thermo Fisher Scientific), and stored in a light-proof box at 4°C before imaging. Multiplexed fluorescent labeled images of one to five randomly selected fields (669 μm by 500 μm) were captured with an automated imaging system (Vectra 3, PerkinElmer). Cell counts were determined manually for each image.

CyTOF analysis
CyTOF staining and analysis were performed as described (*37*). The antibodies used in the CyTOF analyses are summarized in table S4. Cells were subjected to staining after they were washed with phosphate-buffered saline (PBS) supplemented with 2% fetal calf serum (FCS; washing solution) and then with PBS to reduce the protein concentration in the medium, which interferes with the subsequent dead cell staining by cisplatin. The cells were incubated in 5 μM Cell-ID Cisplatin solution (Fluidigm catalog no. 201064, South San Francisco, CA) in PBS, washed using washing solution, and stained with a mixture of surface antibodies. After the cells were

washed, they were fixed and permeabilized using Foxp3/Transcription Factor Staining Buffer Set (Thermo Fisher Scientific) according to the manufacturer's instructions. The fixed and permeabilized cells were then stained with the intracellular antibodies. After the cells were washed twice, they were rested overnight in 125 nM MaxPar Intercalator-Ir (Fluidigm) diluted in 2% paraformaldehyde PBS solution at 4°C. The cells were then washed once with washing solution and twice with MaxPar water (Fluidigm catalog no. 201069), distilled water with minimal heavy element contamination, to reduce the background level. The cells suspended in MaxPar water supplemented with 10% EQ Four Element Calibration Beads (Fluidigm) were applied to the Helios instrument (Fluidigm), and data were acquired at a speed below 300 events/s.

Flow cytometry analysis
Flow cytometry staining and analysis were performed as described (37). The antibodies used in the flow cytometry analyses are summarized in table S5. Cells were washed using washing solution and subjected to staining with surface antibodies. Intracellular staining of FOXP3, pJAK2, and pSTAT5 was performed with anti-Foxp3 mAb, anti-pJAK2 mAb, and anti-pSTAT5 mAb and the Foxp3/ Transcription Factor Staining Buffer Set (Thermo Fisher Scientific) according to the manufacturer's instructions. After the cells were washed, they were analyzed with an LSRFortessa or FACSymphony (BD Biosciences, Franklin Lakes, NJ) and FlowJo software (TreeStar, Ashland, OR). The staining antibodies were diluted according to the manufacturer's instructions.

RNA sequencing
After quality assessment with an Agilent 2100 Bioanalyzer (Agilent Technologies, Santa Clara, CA), polyadenylated RNA libraries were generated using a TruSeq Stranded mRNA Sample Prep Kit (Illumina, San Diego, CA) on an Agilent XT-Auto System (Agilent Technologies) and sequenced with a HiSeq SBS Kit v4-HS (Illumina) on HiSeq2500 (Illumina). Sequence data were evaluated with GeneData Expressionist for Genomic Profiling (version 9.1.4a). Read mapping was performed with Hg19 as the reference genome and TopHat (version 2.0.14), followed by transcriptome reconstruction and expression quantification into fragments per kilobase of transcript model per million (FPKM).

Whole-exome sequencing and mutational analysis
DNA libraries were established with a SureSelect XT Human All Exon system (Agilent Technologies) and sequenced with a HiSeq SBS Kit v4-HS (Illumina) on a HiSeq2500 system (Illumina) to generate paired-end reads (2×100 base pairs). Sequence alignment and mutation calling were performed using the Genomon pipeline (https:// github.com/Genomon-Project/), as described previously (38). Candidate mutations were detected by the Empirical Bayesian Mutation Calling (EBCall) algorithm, and those with (i) a P value $<10^{-4}$, (ii) >4 variant reads in tumor samples, and (iii) a variant allele frequency (VAF) value in tumor samples of >0.025 were adopted. These candidate mutations were further filtered by excluding (i) synonymous single-nucleotide variants; (ii) known variants listed in the 1000 Genomes Project (October 2014 release), National Center for Biotechnology Information (NCBI) dbSNP build 131, National Heart, Lung, and Blood Institute Exome Sequencing Project 6500, Human Genome Variation Database, or our in-house single-nucleotide polymorphism database; and (iii) variants present only in unidirectional reads.

Gene expression data analysis
In addition to our RNA-seq dataset, a TCGA dataset of LUADs was also analyzed. The *EGFR* gene status and mutation burden for 230 LUADs were evaluated on the basis of previously published reports, and gene expression profiles and nonsynonymous mutations of these samples were extracted from the TCGA data portal (https:// tcga-data.nci.nih.gov/tcga/tcgaHome2.jsp). For clustering, we used Cluster 3 for CD4^{+} T_{reg}, CD8^{+} T cell, macrophage, DC, MHC class I cell, costimulatory APC and T cell, coinhibitory APC and T cell, type I IFN response, type II IFN response, and cytolytic activity gene sets as previously reported (12).

Gene set enrichment analysis
GSEA was carried out to analyze the differences between two groups: activated EGFR signaling and inhibited EGFR signaling in three lung cancer cell lines (PC-9, HCC827, and H322). The gene sets were adopted from The Molecular Signatures Database. The phenotype label was EGFR activation score versus EGFR inhibition score.

Gene expression analysis using the nCounter platform
For RNA purification, 10-μm formalin-fixed, paraffin-embedded slides were used for each tumor specimen. RNA was extracted using the RecoverAll Total Nucleic Acid Isolation Kit (Thermo Fisher Scientific). A minimum of 100 ng of total RNA was used to measure chemokine expression. Gene expression analyses were performed using the Human PanCancer IO 360 Panel and nCounter Low RNA Input Kit (Nanostring Technologies, Seattle, WA). Data were normalized by nSolver analysis software.

Cell line and reagents
A549, H322, and HCC827 cells (human NSCLC cell lines) were obtained from American Type Culture Collection (ATCC; Manassas, VA) (ATCC catalog no. CRL-7909, catalog no. CRL-5806, and catalog no. CRL-2868, respectively), and PC-9 cell line (human NSCLC cell line) was obtained from the European Collection of Authenticated Cell Cultures (ECACC) (Salisbury, UK) (ECACC catalog no. 90071810). MC-38 cell line (mouse colon cancer cell line) was obtained from Kerafast (Boston, MA) (catalog no. ENH204), and LL/2 cell line (mouse lung cancer cell line) was obtained from ATCC (ATCC catalog no. CRL-1642). All human cell lines were authenticated using a short tandem repeat DNA method. The A549 and LL/2 cell lines were maintained in Dulbecco's modified Eagle's medium (FUJIFILM Wako Pure Chemical Corporation, Osaka, Japan) supplemented with 10% FCS. The H322, HCC827, and MC-38 cell lines were maintained in RPMI medium (FUJIFILM Wako Pure Chemical Corporation) supplemented with 10% FCS. The human *EGFR* (wild type or exon 19 deletion)–overexpressing MC-38 and LL/2-OVA cell lines were established retrovirally using a pBabe-puro vector (Addgene, Cambridge, MA) (named MC-38wt, MC-38ex19del, LL/2-OVAwt, and LL/2-OVAex19del cell lines). Erlotinib was obtained from Cayman Chemical Company (Ann Arbor, MI), osimertinib was purchased from Selleck (Houston, TX), anti-mouse PD-1 mAb was provided by Ono Pharmaceutical (Osaka, Japan), anti-mouse CXCL10 mAb (clone 134013, R&D Systems, catalog no. MAB466–100) and anti-mouse CCL22 mAb (clone 158132, R&D Systems, catalog no. AF439) were obtained from R&D Systems (Minneapolis, MN), and anti-mouse CD25 (clone PC61, Biolegend, catalog no. 102040) was purchased from BioLegend (San Diego, CA). IFN-γ and EGF were purchased from PeproTech (Rocky Hill, NJ).

qRT-PCR and microarray analyses

Total RNA was reverse-transcribed to complementary DNA using a SuperScript VILO Master Mix according to the manufacturer's instructions (Thermo Fisher Scientific), and real-time PCR was performed with PowerUp SYBR (Thermo Fisher Scientific). The glyceraldehyde-3-phosphate dehydrogenase gene was used as an endogenous control, and the primers used are summarized in table S6. Microarray analysis was performed using the Clariom S array according to the manufacturer's instructions (Thermo Fisher Scientific).

Enzyme-linked immunosorbent assay

The concentrations of CXCL10 and CCL22 were examined with a specific sandwich ELISA according to the manufacturer's instructions (R&D Systems).

Western blotting

Subconfluent cells were washed with PBS and harvested with mammalian protein extraction reagent (M-PER) (Thermo Fisher Scientific). Whole-cell extracts were separated with SDS–polyacrylamide gel electrophoresis and were blotted onto a polyvinylidene fluoride membrane. After the membrane was blocked, it was probed with the primary antibody. After the membrane was rinsed twice with tris-buffered saline buffer, it was incubated with a horseradish peroxidase–conjugated secondary antibody and washed, followed by visualization using an enhanced chemiluminesence detection system and a LAS-4000 (GE Healthcare). The antibodies used in Western blot analyses are summarized in table S7.

Small interfering RNA

Cells were transfected with a small interfering RNA (siRNA) for *JUN* or *IRF1* and a nonspecific target (control) using RNAiMAX (Thermo Fisher Scientific). ON-TARGETplus Human *JUN* siRNA SMART pool (Dharmacon catalog no. L-003268-00-0005, Lafayette, CO), ON-TARGETplus Human *IRF1* siRNA SMART pool (Dharmacon catalog no. L-011704-00-0005), and ON-TARGETplus Non-targeting Pool (Dharmacon catalog no. D-001810-1005) were used.

Luciferase assay

A pNL2.1 vector (Promega catalog no. N1061, Madison, WI) containing the *CXCL10* or *CCL22* promoter region upstream of the luciferase gene was generated. Luciferase activity was determined using the Luciferase Assay System (Promega). The results are reported as the fold induction compared with the control group.

In vivo animal model

C57BL/6 mice (6-week-old females; CLEA Japan, Tokyo, Japan) were used for the in vivo studies. Animal care and experiments were conducted according to the guidelines established by the animal committee of the National Cancer Center after approval of the Ethics Review Committee for Animal Experimentation of the National Cancer Center. A suspension of 1×10^6 transfected cells (in 100 µl of PBS) was subcutaneously (MC-38) or intravenously (LL/2-OVA) administered, and treatment was started after 1 week, when tumors in each group reached an average volume of about 500 mm^3. In some groups, anti–PD-1 mAb (200 µg per body intraperitoneally) was administered at 1-week intervals with or without oral daily erlotinib (30 mg/kg) for 3 weeks. The tumor volume was assessed twice a week as the length × width^2 × 0.5. For blocking of CXCL10 and CCL22, 50 µg of anti-mouse CXCL10 mAb and 20 µg of anti-mouse CCL22 mAb, respectively, were administered intraperitoneally on days 4 and 7 after tumor implantation. For depletion of T$_{regs}$, 200 µg of anti-mouse CD25 mAb was administered intraperitoneally on day 7 after tumor implantation. TIL analysis was performed on day 10.

WST1 assay

The WST1 assay was performed according to the manufacturer's instructions (Roche, Basel, CH) to evaluate the sensitivities to erlotinib and cell proliferation. After each cell line was seeded in a 96-well plate, the cells were incubated with erlotinib for 48 hours. Then, WST1 reagent (10% of medium) was added, and absorbance was analyzed by a microplate reader at 450 and 690 nm. The proliferation of the transfected MC-38 cell lines was analyzed in the same way without erlotinib 0, 24, and 48 hours after seeding.

Statistical analysis

Continuous variables were analyzed with Welch's or paired *t* tests. Survival curves were estimated with the Kaplan-Meier method and compared with the log-rank test. The statistical analyses were performed with Prism version 7 software (GraphPad Software Inc., La Jolla, CA). A *P* value of less than 0.05 was considered statistically significant.

SUPPLEMENTARY MATERIALS

View/request a protocol for this paper from *Bio-protocol*.

REFERENCES AND NOTES

1. T. S. Mok, Y.-L. Wu, S. Thongprasert, C.-H. Yang, D.-T. Chu, N. Saijo, P. Sunpaweravong, B. Han, B. Margono, Y. Ichinose, Y. Nishiwaki, Y. Ohe, J. J. Yang, B. Chewaskulyong, H. Jiang, E. L. Duffield, C. L. Watkins, A. A. Armour, M. Fukuoka, Gefitinib or carboplatin–paclitaxel in pulmonary adenocarcinoma. *N. Engl. J. Med.* **361**, 947–957 (2009).

2. E. L. Kwak, Y.-J. Bang, D. R. Camidge, A. T. Shaw, B. Solomon, R. G. Maki, S.-H. Ou, B. J. Dezube, P. A. Jänne, D. B. Costa, M. Varella-Garcia, W.-H. Kim, T. J. Lynch, P. Fidias, H. Stubbs, J. A. Engelman, L. V. Sequist, W. Tan, L. Gandhi, M. Mino-Kenudson, G. C. Wei, S. M. Shreeve, M. J. Ratain, J. Settleman, J. G. Christensen, D. A. Haber, K. Wilner, R. Salgia, G. I. Shapiro, J. W. Clark, A. J. Iafrate, Anaplastic lymphoma kinase inhibition in non–small-cell lung cancer. *N. Engl. J. Med.* **363**, 1693–1703 (2010).

3. T. Mitsudomi, Y. Yatabe, Mutations of the epidermal growth factor receptor gene and related genes as determinants of epidermal growth factor receptor tyrosine kinase inhibitors sensitivity in lung cancer. *Cancer Sci.* **98**, 1817–1824 (2007).

4. H. Borghaei, L. Paz-Ares, L. Horn, D. R. Spigel, M. Steins, N. E. Ready, L. Q. Chow, E. E. Vokes, E. Felip, E. Holgado, F. Barlesi, M. Kohlhäufl, O. Arrieta, M. A. Burgio, J. Fayette, H. Lena, E. Poddubskaya, D. E. Gerber, S. N. Gettinger, C. M. Rudin, N. Rizvi, L. Crinò, G. R. Blumenschein Jr., S. J. Antonia, C. Dorange, C. T. Harbison, F. Graf Finckenstein, J. R. Brahmer, Nivolumab versus docetaxel in advanced nonsquamous non–small-cell lung cancer. *N. Engl. J. Med.* **373**, 1627–1639 (2015).

5. M. Reck, D. Rodríguez-Abreu, A. G. Robinson, R. Hui, T. Csőszi, A. Fülöp, M. Gottfried, N. Peled, A. Tafreshi, S. Cuffe, M. O'Brien, S. Rao, K. Hotta, M. A. Leiby, G. M. Lubiniecki, Y. Shentu, R. Rangwala, J. R. Brahmer; KEYNOTE-024 Investigators, Pembrolizumab versus chemotherapy for pd-l1–positive non–small-cell lung cancer. *N. Engl. J. Med.* **375**, 1823–1833 (2016).

6. W. Zou, J. D. Wolchok, L. Chen, PD-L1 (B7-H1) and PD-1 pathway blockade for cancer therapy: Mechanisms, response biomarkers, and combinations. *Sci. Transl. Med.* **8**, 328rv324 (2016).

7. J. F. Gainor, A. T. Shaw, L. V. Sequist, X. Fu, C. G. Azzoli, Z. Piotrowska, T. G. Huynh, L. Zhao, L. Fulton, K. R. Schultz, E. Howe, A. F. Farago, R. J. Sullivan, J. R. Stone, S. Digumarthy, T. Moran, A. N. Hata, Y. Yagi, B. Y. Yeap, J. A. Engelman, M. Mino-Kenudson, EGFR mutations and ALK rearrangements are associated with low response rates to PD-1 pathway blockade in non–small cell lung cancer: A retrospective analysis. *Clin. Cancer Res.* **22**, 4585–4593 (2016).

8. C. K. Lee, J. Man, S. Lord, M. Links, V. Gebski, T. Mok, J. C. Yang, Checkpoint inhibitors in metastatic *EGFR*-mutated non-small cell lung cancer—A meta-analysis. *J. Thorac. Oncol.* **12**, 403–407 (2017).

9. K. Azuma, K. Ota, A. Kawahara, S. Hattori, E. Iwama, T. Harada, K. Matsumoto, K. Takayama, S. Takamori, M. Kage, T. Hoshino, Y. Nakanishi, I. Okamoto, Association of PD-L1 overexpression with activating EGFR mutations in surgically resected nonsmall-cell lung cancer. *Ann. Oncol.* **25**, 1935–1940 (2014).

10. N. Chen, W. Fang, J. Zhan, S. Hong, Y. Tang, S. Kang, Y. Zhang, X. He, T. Zhou, T. Qin, Y. Huang, X. Yi, L. Zhang, Upregulation of PD-L1 by EGFR activation mediates the immune escape in EGFR-driven NSCLC: Implication for optional immune targeted therapy for NSCLC patients with EGFR mutation. *J. Thorac. Oncol.* **10**, 910–923 (2015).

11. N. A. Rizvi, M. D. Hellmann, A. Snyder, P. Kvistborg, V. Makarov, J. J. Havel, W. Lee, J. Yuan, P. Wong, T. S. Ho, M. L. Miller, N. Rekhtman, A. L. Moreira, F. Ibrahim, C. Bruggeman, B. Gasmi, R. Zappasodi, Y. Maeda, C. Sander, E. B. Garon, T. Merghoub, J. D. Wolchok, T. N. Schumacher, T. A. Chan, Mutational landscape determines sensitivity to PD-1 blockade in non–small cell lung cancer. *Science* **348**, 124–128 (2015).

12. M. S. Rooney, S. A. Shukla, C. J. Wu, G. Getz, N. Hacohen, Molecular and genetic properties of tumors associated with local immune cytolytic activity. *Cell* **160**, 48–61 (2015).

13. M. Saito, Y. Shimada, K. Shiraishi, H. Sakamoto, K. Tsuta, H. Totsuka, S. Chiku, H. Ichikawa, M. Kato, S.-i. Watanabe, T. Yoshida, J. Yokota, T. Kohno, Development of lung adenocarcinomas with exclusive dependence on oncogene fusions. *Cancer Res.* **75**, 2264–2271 (2015).

14. S. L. Topalian, C. G. Drake, D. M. Pardoll, Immune checkpoint blockade: A common denominator approach to cancer therapy. *Cancer Cell* **27**, 450–461 (2015).

15. S. Spranger, R. M. Spaapen, Y. Zha, J. Williams, Y. Meng, T. T. Ha, T. F. Gajewski, Up-regulation of PD-L1, IDO, and T_regs in the melanoma tumor microenvironment is driven by CD8$^+$ T cells. *Sci. Transl. Med.* **5**, 200ra116 (2013).

16. D. Q. Tran, H. Ramsey, E. M. Shevach, Induction of FOXP3 expression in naive human CD4$^+$FOXP3$^-$ T cells by T-cell receptor stimulation is transforming growth factor-β–dependent but does not confer a regulatory phenotype. *Blood* **110**, 2983–2990 (2007).

17. M. Miyara, Y. Yoshioka, A. Kitoh, T. Shima, K. Wing, A. Niwa, C. Parizot, C. Taflin, T. Heike, D. Valeyre, A. Mathian, T. Nakahata, T. Yamaguchi, T. Nomura, M. Ono, Z. Amoura, G. Gorochov, S. Sakaguchi, Functional delineation and differentiation dynamics of human CD4$^+$ T cells expressing the FoxP3 transcription factor. *Immunity* **30**, 899–911 (2009).

18. T. Saito, H. Nishikawa, H. Wada, Y. Nagano, D. Sugiyama, K. Atarashi, Y. Maeda, M. Hamaguchi, N. Ohkura, E. Sato, H. Nagase, J. Nishimura, H. Yamamoto, S. Takiguchi, T. Tanoue, W. Suda, H. Morita, M. Hattori, K. Honda, M. Mori, Y. Doki, S. Sakaguchi, Two FOXP3$^+$CD4$^+$ T cell subpopulations distinctly control the prognosis of colorectal cancers. *Nat. Med.* **22**, 679–684 (2016).

19. Y. Togashi, H. Nishikawa, Regulatory T Cells: Molecular and Cellular Basis for Immunoregulation. *Curr. Top. Microbiol. Immunol.* **410**, 3–27 (2017).

20. K. Van Raemdonck, P. E. Van den Steen, S. Liekens, J. Van Damme, S. Struyf, CXCR3 ligands in disease and therapy. *Cytokine Growth Factor Rev.* **26**, 311–327 (2015).

21. D. Peng, I. Kryczek, N. Nagarsheth, L. Zhao, S. Wei, W. Wang, Y. Sun, E. Zhao, L. Vatan, W. Szeliga, J. Kotarski, R. Tarkowski, Y. Dou, K. Cho, S. Hensley-Alford, A. Munkarah, R. Liu, W. Zou, Epigenetic silencing of T_H1-type chemokines shapes tumour immunity and immunotherapy. *Nature* **527**, 249–253 (2015).

22. O. Yoshie, K. Matsushima, CCR4 and its ligands: From bench to bedside. *Int. Immunol.* **27**, 11–20 (2015).

23. T. J. Curiel, G. Coukos, L. Zou, X. Alvarez, P. Cheng, P. Mottram, M. Evdemon-Hogan, J. R. Conejo-Garcia, L. Zhang, M. Burow, Y. Zhu, S. Wei, I. Kryczek, B. Daniel, A. Gordon, L. Myers, A. Lackner, M. L. Disis, K. L. Knutson, L. Chen, W. Zou, Specific recruitment of regulatory T cells in ovarian carcinoma fosters immune privilege and predicts reduced survival. *Nat. Med.* **10**, 942–949 (2004).

24. D. Liang, H. Xiao-Feng, D. Guan-Jun, H. Er-Ling, C. Sheng, W. Ting-Ting, H. Qin-Gang, N. Yan-Hong, H. Ya-Yi, Activated STING enhances Tregs infiltration in the HPV-related carcinogenesis of tongue squamous cells via the c-jun/CCL22 signal. *Biochim. Biophys. Acta* **1852**, 2494–2503 (2015).

25. P.-C. Tseng, C.-L. Chen, Y.-S. Shan, C.-F. Lin, An increase in galectin-3 causes cellular unresponsiveness to IFN-γ–induced signal transduction and growth inhibition in gastric cancer cells. *Oncotarget* **7**, 15150–15160 (2016).

26. S. Matsuzaki, T. Ishizuka, T. Hisada, H. Aoki, M. Komachi, I. Ichimonji, M. Utsugi, A. Ono, Y. Koga, K. Dobashi, H. Kurose, H. Tomura, M. Mori, F. Okajima, Lysophosphatidic acid inhibits CC chemokine ligand 5/RANTES production by blocking IRF-1–mediated gene transcription in human bronchial epithelial cells. *J. Immunol.* **185**, 4863–4872 (2010).

27. F. MacDonald, D. M. W. Zaiss, The immune system's contribution to the clinical efficacy of EGFR antagonist treatment. *Front. Pharmacol.* **8**, 575 (2017).

28. D. M. Zaiss, J. van Loosdregt, A. Gorlani, C. P. Bekker, A. Gröne, M. Sibilia, P. M. van Bergen en Henegouwen, R. C. Roovers, P. J. Coffer, A. J. Sijts, Amphiregulin enhances regulatory T cell-suppressive function via the epidermal growth factor receptor. *Immunity* **38**, 275–284 (2013).

29. N. Nakamura, H. Chin, N. Miyasaka, O. Miura, An epidermal growth factor receptor/Jak2 tyrosine kinase domain chimera induces tyrosine phosphorylation of Stat5 and transduces a growth signal in hematopoietic cells. *J. Biol. Chem.* **271**, 19483–19488 (1996).

30. A. Garcia-Diaz, D. S. Shin, B. H. Moreno, J. Saco, H. Escuin-Ordinas, G. A. Rodriguez, J. M. Zaretsky, L. Sun, W. Hugo, X. Wang, G. Parisi, C. P. Saus, D. Y. Torrejon, T. G. Graeber, B. Comin-Anduix, S. Hu-Lieskovan, R. Damoiseaux, R. S. Lo, A. Ribas, Interferon receptor signaling pathways regulating PD-L1 and PD-L2 expression. *Cell Rep.* **19**, 1189–1201 (2017).

31. M. A. Socinski, R. M. Jotte, F. Cappuzzo, F. Orlandi, D. Stroyakovskiy, N. Nogami, D. Rodríguez-Abreu, D. Moro-Sibilot, C. A. Thomas, F. Barlesi, G. Finley, C. Kelsch, A. Lee, S. Coleman, Y. Deng, Y. Shen, M. Kowanetz, A. Lopez-Chavez, A. Sandler, M. Reck; IMpower150 Study Group, Atezolizumab for first-line treatment of metastatic nonsquamous NSCLC. *N. Engl. J. Med.* **378**, 2288–2301 (2018).

32. T. Voron, E. Marcheteau, S. Pernot, O. Colussi, E. Tartour, J. Taieb, M. Terme, Control of the immune response by pro-angiogenic factors. *Front. Oncol.* **4**, 70 (2014).

33. F. Balkwill, Cancer and the chemokine network. *Nat. Rev. Cancer* **4**, 540–550 (2004).

34. E. Poole, C. A. King, J. H. Sinclair, A. Alcami, The UL144 gene product of human cytomegalovirus activates NFκB via a TRAF6-dependent mechanism. *EMBO J.* **25**, 4390–4399 (2006).

35. N. Dixit, S. I. Simon, Chemokines, selectins and intracellular calcium flux: Temporal and spatial cues for leukocyte arrest. *Front. Immunol.* **3**, 188 (2012).

36. M. D. Gunn, S. Kyuwa, C. Tam, T. Kakiuchi, A. Matsuzawa, L. T. Williams, H. Nakano, Mice lacking expression of secondary lymphoid organ chemokine have defects in lymphocyte homing and dendritic cell localization. *J. Exp. Med.* **189**, 451–460 (1999).

37. Y. Takeuchi, A. Tanemura, Y. Tada, I. Katayama, A. Kumanogoh, H. Nishikawa, Clinical response to PD-1 blockade correlates with a sub-fraction of peripheral central memory CD4$^+$ T cells in patients with malignant melanoma. *Int. Immunol.* **30**, 13–22 (2018).

38. K. Kataoka, Y. Nagata, A. Kitanaka, Y. Shiraishi, T. Shimamura, J.-i. Yasunaga, Y. Totoki, K. Chiba, A. Sato-Otsubo, G. Nagae, R. Ishii, S. Muto, S. Kotani, Y. Watatani, J. Takeda, M. Sanada, H. Tanaka, H. Suzuki, Y. Sato, Y. Shiozawa, T. Yoshizato, K. Yoshida, H. Makishima, M. Iwanaga, G. Ma, K. Nosaka, M. Hishizawa, H. Itonaga, Y. Imaizumi, W. Munakata, H. Ogasawara, T. Sato, K. Sasai, K. Muramoto, M. Penova, T. Kawaguchi, H. Nakamura, N. Hama, K. Shide, Y. Kubuki, T. Hidaka, T. Kameda, T. Nakamaki, K. Ishiyama, S. Miyawaki, S.-S. Yoon, K. Tobinai, Y. Miyazaki, A. Takaori-Kondo, F. Matsuda, K. Takeuchi, O. Nureki, H. Aburatani, T. Watanabe, T. Shibata, M. Matsuoka, S. Miyano, K. Shimoda, S. Ogawa, Integrated molecular analysis of adult T cell leukemia/lymphoma. *Nat. Genet.* **47**, 1304–1315 (2015).

Citation: E. Sugiyama, Y. Togashi, Y. Takeuchi, S. Shinya, Y. Tada, K. Kataoka, K. Tane, E. Sato, G. Ishii, K. Goto, Y. Shintani, M. Okumura, M. Tsuboi, H. Nishikawa, Blockade of EGFR improves responsiveness to PD-1 blockade in *EGFR*-mutated non–small cell lung cancer. *Sci. Immunol.* **5**, eaav3937 (2020).

Science Immunology

Blockade of EGFR improves responsiveness to PD-1 blockade in *EGFR*-mutated non−small cell lung cancer

Eri Sugiyama, Yosuke Togashi, Yoshiko Takeuchi, Sayoko Shinya, Yasuko Tada, Keisuke Kataoka, Kenta Tane, Eiichi Sato, Genichiro Ishii, Koichi Goto, Yasushi Shintani, Meinoshin Okumura, Masahiro Tsuboi and Hiroyoshi Nishikawa

Giving anti−PD-1 a boost

Anti−PD-1 therapy is ineffective in the context of *EGFR*-mutated lung adenocarcinomas. Here, Sugiyama *et al.* find that these tumors have an immunosuppressive tumor microenvironment characterized by increased infiltration of regulatory T cells. Using a mouse model, the Sugiyama *et al.* demonstrate that a clinically available EGFR inhibitor, erlotinib, can be used improve responsiveness to anti−PD-1 therapy in *EGFR*-mutated LDACs. Because both anti−PD-1 antibodies and erolitinib are already being used in the clinic, this preclinical proof-of-concept study should serve as a basis for clinical studies to examine whether erolitnib enhances responsiveness of *EGFR*-mutated lung adenocarcinomas to PD-1 −centric therapies.

ARTICLE TOOLS	http://immunology.sciencemag.org/content/5/43/eaav3937
SUPPLEMENTARY MATERIALS	http://immunology.sciencemag.org/content/suppl/2020/01/27/5.43.eaav3937.DC1
REFERENCES	This article cites 38 articles, 9 of which you can access for free http://immunology.sciencemag.org/content/5/43/eaav3937#BIBL

Use of this article is subject to the Terms of Service